Liquid Crystals
Publication details, including instructions for authors and subscription information:
http://www.informaworld.com/smpp/title~content=t713926090

Mixture of changing uniaxial micellar forms in lyotropic biaxial nematics

E. F. Henriques[a]; C. B. Passos[a]; V. B. Henriques[b]; L. Q. Amaral[b]
[a] Instituto de Física e Matemática, Universidade Federal de Pelotas, 96010-900 Pelotas, RS, Brasil [b] Instituto de Física, Universidade de São Paulo, 05389-970 São Paulo, SP, Brasil

To cite this Article Henriques, E. F. , Passos, C. B. , Henriques, V. B. and Amaral, L. Q.(2008) 'Mixture of changing uniaxial micellar forms in lyotropic biaxial nematics', Liquid Crystals, 35: 5, 555 — 568
To link to this Article: DOI: 10.1080/02678290802015986
URL: http://dx.doi.org/10.1080/02678290802015986

Liquid Crystals,
Vol. 35, No. 5, May 2008, 555–568

Taylor & Francis
Taylor & Francis Group

Mixture of changing uniaxial micellar forms in lyotropic biaxial nematics

E. F. Henriques[a]*, C. B. Passos[a], V. B. Henriques[b] and L. Q. Amaral[b]

[a]*Instituto de Física e Matemática, Universidade Federal de Pelotas, Caixa Postal 354, 96010-900 Pelotas, RS, Brasil;* [b]*Instituto de Física, Universidade de São Paulo, Caixa Postal 66318, 05389-970 São Paulo, SP, Brasil*

(16 January 2007; final form 8 February 2008)

Lyotropic nematics consisting of surfactant–cosurfactant water solutions may present a biaxial phase or direct $U(+)\leftrightarrow U(-)$ transitions, in different regions of the temperature-relative concentration phase diagram, for different systems and compositions. We propose that these may be related to changes of uniaxial micellar form, which may occur either smoothly or abruptly. Smooth change of cylinder-like into disc-like shapes requires a distribution of Maier–Saupe interaction constants and we consider two limiting cases for the distribution of forms: a single Gaussian and a double Gaussian. Alternatively, an abrupt change of form is described by a discontinuous distribution of interaction constants. Our results show that the dispersive distributions yield a biaxial phase, while an abrupt change of shape leads to coexistence of uniaxial phases. Fitting the theory to the experiment for the ternary system KL/decanol/D_2O leads to transition lines in very good agreement with experimental results. In order to rationalise the results of the comparison, we analyse temperature and concentration form dependence, which connects micellar and experimental macroscopic parameters. Physically consistent variations of micellar asymmetry, amphiphile partitioning and volume are obtained. To the best of the authors' knowledge, this is the first truly statistical microscopic approach that is able to model experimentally observed lyotropic biaxial nematic phases.

Keywords: biaxial nematics; statistical model; mixing and phase separation; micelle form

1. Introduction

The symmetry of nuclear magnetic resonance (NMR) and X-ray diffraction results on oriented lyotropic nematic phases in amphiphile/water/additive systems has led to the proposal of micelles of cylindrical form in N_C phases or discotic form in N_D phases (*1–3*). The nematic N_C domain usually occurs near a hexagonal phase, with the N_D region near a lamellar phase. The hexagonal and lamellar phases are made of, respectively, cylindrical micelles and planar bilayer aggregates (*4, 5*).

The discovery of a biaxial nematic lyomesophase N_{bx} in the potassium laurate (KL)/D_2O/decanol system (*6*), between lyotropic nematic phases with diamagnetic and optical anisotropies of opposite sign near a re-entrant isotropic phase (*6*), created doubts regarding the form and symmetry of the micellar objects (*7, 8*).

The search for thermotropic biaxial phases was initially unsuccessful, but recently there has been strong indications that thermotropic biaxial phases may exist (*9*). Biaxial molecular systems, such as side-chain polymer (*10*), non-linear molecules of boomerang types (*11, 12*) and organo siloxane tetrapodes (*13*) were reported to exhibit biaxial phases.

Before the discovery of the lyotropic biaxial phase, theoretical papers predicted the existence of a biaxial nematic phase for systems of biaxially symmetrical molecules interacting either through soft Maier–Saupe energy (*14, 15*) or via the hard Onsager interactions (*16, 17*). Freiser's initial proposal of a biaxial phase for particles of low symmetry was soon followed by the idea that mixtures of plate-like and rod-like molecules (*18*) could also be responsible for biaxial phases. However, in a large number of cases, the biaxial phase proved to be unstable against demixing of the particles of two different shapes (*19–23*), leading to phase coexistence of an N_C and an N_D phase.

Earlier Landau theory (*24*) developed for the nematic–isotropic transition was generalised to include the possibility of axial anisotropies of different sign (*25, 26*) and yielded phase diagrams of different topologies, in which two uniaxial phases may coexist or be separated by an intermediary biaxial phase. Both cases occur in lyotropic systems (*27*). However, Landau theory is based on arguments of symmetry for the macroscopic tensor order parameter (*28*), and cannot by itself identify the relevant physical parameters, such as temperature, pressure or concentration. Those are implicit in the coefficients of the expansion, and cannot be established in the absence of a microscopic statistical theory (*26*). Thus, Landau theory is unable to distinguish between the two possibilities for the

*Corresponding author. Email: efontes@ufpel.edu.br

ISSN 0267-8292 print/ISSN 1366-5855 online

DOI: 10.1080/02678290802015986
http://www.informaworld.com

origin of the biaxial phase: biaxial particles or mixtures of uniaxial particles.

Although mesogenic molecules may deviate from cylindrical symmetry, this is not enough to lead to biaxial phases, since in most cases the uniaxial nematic phase is expected to freeze before the transition to the biaxial nematic can occur (*29*). For thin films, the surface can induce an optical biaxiality in the sample, even if the bulk phase is uniaxial. Many compounds, which showed biaxiality in conoscopy, proved to be uniaxial in the bulk when observed with NMR spectroscopy (*29*).

Statistical microscopic theories that are under consideration to explain the recently observed thermotropic biaxial phases take biaxial molecules interacting via orientational intermolecular potentials (*26, 31, 32*). An important point to note is that, in the thermotropic biaxial nematics, no observation is made of axiality rotation of the nematic phases, as is the case in lyotropic systems (*6, 10–13*, *30*). Thus, the discovery of thermotropic biaxial phases for compounds of molecules with no axial symmetry brings back the question of the origin of biaxiality in lyotropics, since micelles do not have that same intrinsic biaxiality as new biaxial molecules.

Molecular-phenomenological theories focused on lyotropics, with fixed object symmetry (*33*), were able to simulate several aspects of the experimental phase diagrams, of either cylindrical or discotic objects, particularly the transitions from uniaxial nematic N_C and N_D phases to related phases with positional order. This is achieved by taking into account the aggregation process. However, the N_C and N_D phases are never present at the same time in such phase diagrams.

On the other hand, re-entrant behaviour of the nematic into the isotropic phase, as in KL, is impossible to rationalise without temperature effects on the form of the micellar object (*34*). A change of form with temperature may also be expected to occur in the transformation process of cylinders into discs.

The diversity of the experimental lyotropic phases is a challenge to molecular theories. The existence of first-order N_C–N_D transitions in sodium decyl (SDS) and dodecyl (SLS) sulfate/water/decanol, for instance, gives a strong indication (*27*) that micelles are changing form. It was shown by Amaral and colleagues (*35, 36*) that the N_C–N_D transition for these three systems (KL, SDS and SLS) takes place at essentially the same decanol/amphiphile molar ratio. In the more diluted isotropic phase, it was shown that the addition of decanol promotes change of micellar form, from cylinder-like to disc-like, at about the same decanol/SLS molar ratio (*37*). It was later shown that the system SLS sulfate/decanol/water also presents two small biaxial islands of opposed magnetic alignment between the N_C and N_D domain in the concentration versus temperature phase diagram, denoted by N_{bx}^{+} and N_{bx}^{-} (see (*38*)). In the latter case, the phase transitions were concluded to be first order. Biaxial phases have been reported in other lyotropic ternary systems, as in the SLS/hexadecanol/water system (*39*). The system tetra decyltrimethyl ammonium bromide/*n*-decanol/water also shows two distinct biaxial nematic mesophases with opposite diamagnetic and optical anisotropies (*40*).

Lyotropic biaxial phases have bulk biaxiality, as detected by deuterium NMR spectroscopy in static and dynamic measurements in the system KL/decylammonium hydrochloride/water (*41*). A recent work on the temperature dependence of refractive indexes in the (KL)/D_2O/decanol system revealed values compatible with the biaxial phase corresponding to a mixture of the two uniaxial forms (*42*).

The phase sequence N_D–N_{bx}–N_C with decreasing relative cosurfactant concentration values, at fixed temperature, is doubtless correlated with a change between two uniaxial forms. A micelle shape transformation from cylindrical to planar form, as a function of increase in relative co-surfactant concentration, has been modelled in terms of the elastic bending energy due to micelle curvature (*36*), since the tendency of decanol molecules to prefer less curved surfaces is well known (*43*).

To model the the complementary phase sequence N_D–N_{bx}–N_C with temperature, at fixed relative concentrations, we propose that, in this region, micelles are changing form. This change of form may be either smooth or abrupt. In the first case, a homogeneous mixture of cylinders and discs will be present. Phase separation of the aggregates of different geometry is prevented precisely by the fact that forms are in exchange condition in the biaxial phase.

In a previous paper (*44*), a homogeneously distributed mixture of uniaxial micelles of forms ranging from discs to cylinders was modelled using soft quadrupolar interactions with a continuous single Gaussian distribution of quasi-quadrupoles. The theory yields an intermediary stable biaxial phase in the region of small *average* anisometry. The biaxial phase is a result of the mixture in the Gaussian distribution with small mean anisometry. Demixing is prevented by the spatial homogeneity of the random distribution of forms.

In this study, we generalise our previous approach in order to include the possibilities of abrupt or continuous change of form. Qualitative comparison with the experimental phase diagram of Yu and Saupe (*6*), as well as SDS/water/decanol systems displaying no biaxial phase, can then be undertaken. In the former

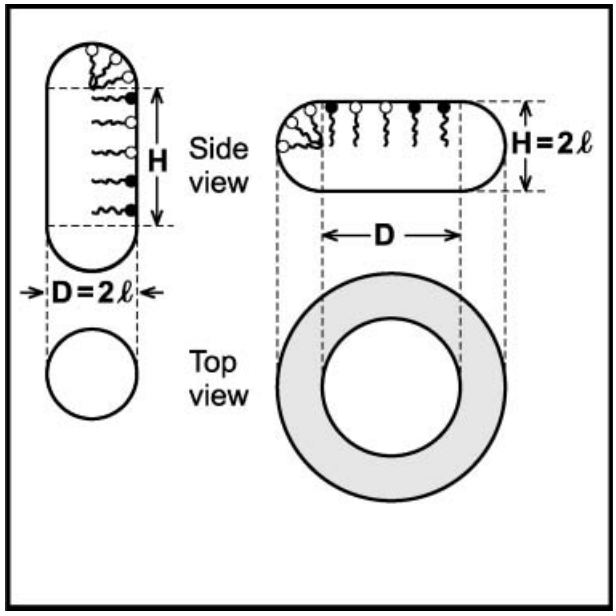

Figure 1. Geometrical models of the micelles: l is a fixed mean hydrocarbon chain length for a given temperature; $v=H/D$ is defined for both shapes.

case, we were also able to present a quantitative comparison from a micellar standpoint, adopting explicit geometric models for the micelles and form change according to partitioning of the surfactant, in the spirit of the work of Amaral and colleagues (*36*).

This article is organised as follows. The statistical model is presented in section 2. Results for the chosen quadrupole distributions are shown in section 3. Comparisons between the experimental and theoretical phase diagrams are presented in section 4, through simple linear fitting of the model parameters. The model allows determination of the numerical phase biaxiality, and a discussion of the extent to which these might be compared with experimental values from the literature is given. In section 5, the theoretical results are interpreted within the adopted geometric modelling for the aggregates. Final comments are given in section 6.

2. The model

Amphiphile molecules in solution spontaneously aggregate into thermodynamically stable micelles and bilayers (*45*), with forms depending on the geometry of the molecules (*46*).

As discussed in the introduction, experimental and theoretical studies evidence that micelles in ternary systems amphiphile/decanol/water may change form as a function of relative concentration, because decanol favours flatness of the interfaces. Both amphiphile and decanol are within the micellar aggregate and a change in form occurs with rearrangements of molecules inside the micelle. However, a complete theory of micelle transformation is not yet available.

In this paper the existence of micelles of two uniaxial forms, spherocylinders and discs (Figure 1), is postulated, but the micelles are changing form, size and aggregation number. In order to represent the change of form from cylinders to discs, under variations of temperature T or relative concentration P, we admit two possibilities: a smooth transformation of form of a polydisperse solution, or an abrupt change of monodisperse form. Therefore, we consider a dispersion of uniaxial particles (micelles themselves, not their constituent molecules), which presents a distribution of anisometries μ_i that interact through an orientational potential. The distributions are necessarily *ad-hoc* because the form changing process itself cannot be modelled. It should be stressed that our model is not analogous to either mixtures of fixed forms or flexible molecules.

2.1. *Energy*

Two particles i and j interact with energy (*15, 47*)

$$E_{ij} = -(3/4)\phi(r_{ij})\lambda_i\lambda_j\left[3(\tilde{\mathbf{n}}_i\cdot\tilde{\mathbf{n}}_j)^2-1\right], \qquad (1)$$

where λ_i represents the particle quadrupole (which depends on anisometry μ_i) and $\tilde{\mathbf{n}}_i$ represents the direction vector of symmetry of the uniaxial particle i. The dispersion may include particles of different shapes. Objects with $\lambda_i>0$ are spherocylinders, whereas particles with $\lambda_i<0$ have the form of rounded discs (see Figure 1) (*44*). Thus, in order to lower the energy, two cylinders (or discs) tend to be parallel, whereas a disc and a cylinder tend to align orthogonally.

The overall energy of the system, for a particular distribution of anisometries, is given by

$$E=(\{\lambda_i\},\{\tilde{\mathbf{n}}_i\})=\sum_{(i,j)}E_{i,j}. \qquad (2)$$

Note that the interaction coefficients are not necessarily uniform.

2.2. *Smooth form transformation*

To model a smooth transition of form, we assume a strong dispersion of anisometries in the cylinder–disc transition region, in dynamic equilibrium. In this region, average anisometry should remain small. Accordingly, the system must be described by a set of λ_i. The average form associated to $\lambda_0=\overline{\lambda_i}$ depends on temperature and concentration, i.e. $\lambda_0=\lambda_0(T, P)$.

In the presence of a cylinder–disc mixture, in the transition region, two different possibilities arise:

either (i) relaxation times for micelle form transition disc $\rightleftharpoons$ cylinder is much smaller than the relaxation times for spatial rearrangement of the continuum of disc-like and cylinder-like aggregates, i.e. $\tau_{\text{form distribution}} \ll \tau_{\text{spatial distribution}}$; or, inversely, (ii) $\tau_{\text{form distribution}} \gg \tau_{\text{spatial distribution}}$. In the first situation, form transformation of micelles takes place at much shorter times compared with micelle diffusion, thus yielding a homogeneous mixture. The second case, in which micelle translation occurs at rapid rates, as compared with micelle form transformation, is analogous to a mixture of discs and cylinders of fixed shape, and phase separation is to be expected in most cases (*19, 20, 23*). As the treatment of impurity distribution in solids also displays these two possibilities, we may borrow the corresponding terminology: the first is a ''quenched'' mixture, in which the spatial distribution is frozen in, whereas the second is an ''annealed'' mixture, for which particles may diffuse so as to find an equilibrium distribution (*48, 49*). In our modelling, orientational degrees of freedom are allowed to find an equilibrium distribution for both cases, whereas the spatial distribution is allowed to search for equilibrium only in the annealed case.

Calculation of free energies is very different for the two situations (*48*). In the first case, assuming a dispersion of anisometries described by a certain probability distribution $p(\lambda)$ of quadrupoles, we must calculate the ''quenched'' free energy given by

$$\begin{aligned} F_Q(T, P) &= -k_B T \overline{\ln[Z(T, \{\lambda_i\})]} \\ &= -k_B T \int \left[\prod_i p(\lambda_i) d\lambda_i\right] \ln\left[Z_Q(T, \{\lambda_i\})\right], \end{aligned} \tag{3}$$

where the partition function of a given set $\{\lambda_i\}$ is

$$Z_Q(T, \{\lambda_i\}) = \sum_{\{\tilde{\mathbf{n}}_i\}} \exp\left[-\sum_{(i,j)} \beta E_{i,j}(\{\lambda_i\}, \{\tilde{\mathbf{n}}_i\})\right], \tag{4}$$

with the interaction energy from Equations (1) and (2).

In the second case, the ''annealed'' free energy should be given by

$$F_A(T, P) = -k_B T \ln[Z_A(T, P)], \tag{5}$$

where the ''annealed'' partition function

$$\begin{aligned} Z_A(T, \{\lambda_0(T, P)\}) = \sum_{\{\lambda_i\}} \sum_{\{\tilde{\mathbf{n}}_i\}} \exp\Big[-\sum \beta E_{i,j} \\ (\{\lambda_i\}, \{\tilde{\mathbf{n}}_i\})\Big] \end{aligned} \tag{6}$$

demands a summation over all possible configurations of anisometries $\{\lambda_i\}$, restricted to those leading to a definite average quadrupole $\lambda_0(T, P) = \sum_i \lambda_i / N$, where N is the number of particles. Interaction energy is again taken from Equations (1) and (2).

We assume that smooth micelle form transformation occurs according to the first case. This assumption is suggested by the fact that form transformation is related to molecular diffusion rate, whereas spatial rearrangement is a consequence of micelle diffusion. Thus, in this study, the statistical properties of the model are obtained through Equations (3) and (4).

Different possibilities for the dispersion of micelle form within the solution, described by choices of $p(\lambda)$, were analysed. We have considered a Gaussian distribution

$$p_G(\lambda) = \exp\left[-(\lambda - \lambda_0)^2 \Big/ 2\sigma_0^2\right] \Big/ \sqrt{2\pi}\sigma_0, \tag{7}$$

in which the sign of the mean quadrupole λ_0 indicates the predominance of cylindrical or discotic shape, and a double delta distribution

$$p_\Delta(\lambda) = \delta(\lambda - \lambda_0 - \sigma_0)/2 + \delta(\lambda - \lambda_0 + \sigma_0)/2, \tag{8}$$

which mimics a double Gaussian in a simplified form. In Figure 2, we show different Gaussian distributions with the same average quadrupole λ_0: the top left plot shows a single Gaussian distribution of Equation (7), and the other three plots are double Gaussian distributions with different dispersions. In the top right distribution, each Gaussian has a very small dispersion, similar to double delta distributions of Equation (8). In the bottom left distribution, dispersions are intermediate, so that the two Gaussian functions remain separated; in the bottom right plot, however, dispersions are large, the two Gaussians are indistinguishable and the plot is quantitatively similar to the single Gaussian of the first plot.

2.3. *Abrupt form transformation*

An abrupt cylinder–disc transformation requires a monodisperse micelle solution. This may be described by a discontinuous null dispersion theta distribution

$$p(\lambda) = [1 - \Theta(\lambda + \lambda^*) + \Theta(\lambda - \lambda^*)]\delta(\lambda - \lambda_0). \tag{9}$$

Here, $\lambda^* = \lambda(P, T)$ is some physical limit for λ_0, which may depend on relative concentration P and temperature T. This would correspond to the single Gaussian distribution seen in Figure 2 in the limit of null dispersion. In this case, Equations (3) and (5) lead to identical free energies.

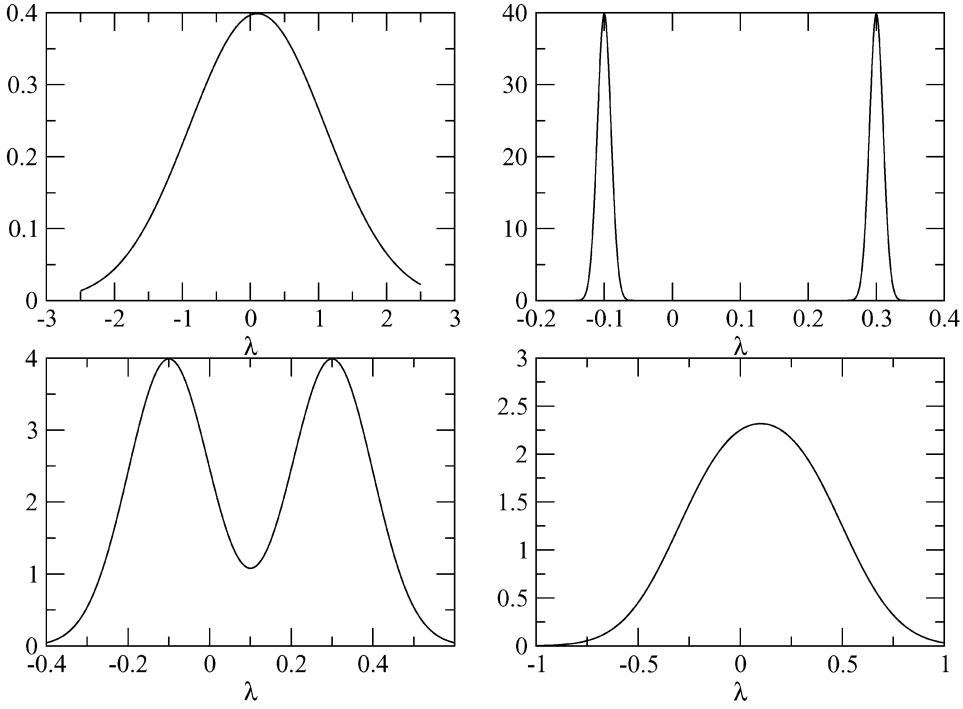

Figure 2. Single Gaussian (top left) and double Gaussian distribution with different dispersion constants and same average mean quadrupole $\lambda_0=0.1$. Gaussians are centered at $\lambda_0=0.1$ (top left), $\lambda_{01}=-0.1$ and $\lambda_{02}=0.3$ (top right and bottom graphs). Dispersions are $\sigma_0=1$ (top left), $\sigma_{01}=\sigma_{02}=0.01$ (top right), $\sigma_{01}=\sigma_{02}=0.1$ (bottom left), $\sigma_{01}=\sigma_{02}=0.25$ (bottom right). The bimodal distribution is obtained in the limit $\sigma_{01}=\sigma_{02}=0$.

3. Order parameters and mean-field Equations

A macroscopic order parameter can be defined in terms of some static response function, such as the anisotropic susceptibility traceless tensor $\widetilde{Q}$. In the simplest situations, this tensor is linearly related to the ordering matrix $\widetilde{S}$ (see (*28*)):

$$\widetilde{S}=\frac{1}{2}\begin{pmatrix} q-m & 0 & 0 \\ 0 & -q-m & 0 \\ 0 & 0 & 2m \end{pmatrix}, \qquad (10)$$

where

$$m=\frac{3}{2}\overline{\left(\langle n_z^2\rangle-1/3\right)} \qquad (11)$$

and

$$q=\frac{3}{2}\overline{\langle n_y^2-n_x^2\rangle}. \qquad (12)$$

Here, n_x, n_y and n_z are the Cartesian components of $\widetilde{\mathbf{n}}_i$. Bars represent averages over $p(\lambda)$ and brackets represent the thermal average. Thus, a uniaxial phase is described by $m\neq 0$ with $q=0$, whereas for the biaxial phase we must have both $m\neq 0$ and $q\neq 0$.

In spite of the microscopic uniaxial symmetry, represented by the particle quadrupole moment $\lambda_{xx}=\lambda_{yy}-\lambda_{zz}/2$, macroscopic biaxiality may arise in the case of the homogeneous mixture, represented by the Gaussian or delta bimodal distribution of forms $p(\lambda)$, Equations (7) and (8), in the transition region.

For simplicity of calculations, we assume that the directions are restricted to one of the three Cartesian axes: $\widetilde{\mathbf{n}}_i=(\pm 1, 0, 0)$, $(0, 0, \pm 1)$ or $(0, \pm 1, 0)$. This has been used in Onsager calculations (*50*), lattice descriptions (*17*) and also in Maier–Saupe models (*34*) and, despite some displacement of entropy variations, does not alter the essential physics of the model. Such a simplification will not hinder comparison with the experimental phase diagram, since we do not seek interpretation of experimental observations that would depend strongly on fluctuational and correlational effects beyond mean-field description, such as critical exponent measurements (*48*).

The mean-field approximation used here is to take $\phi(r_{ij})\sim$constant$/N$ (see (*51*)), which is equivalent to assuming that each micelle interacts with the average orientation of its neighbours. For a particular set of N quadrupoles, $\{\lambda_i\}$, the partition function will be integrable by two Gaussian identities (*52*), giving $Z(T, x, y)$, with x and y given by

$$\frac{x}{J}=\int \lambda p(\lambda)d\lambda\frac{2\sinh\beta(x\lambda)}{e^{-\beta(y\lambda)}+2\cosh\beta(x\lambda)} \qquad (13)$$

and

$$\frac{y}{3J}+\frac{2\lambda_0}{3}=\int \lambda p(\lambda)d\lambda \frac{2\cosh\,\beta(x\lambda)}{e^{-\beta(y\lambda)}+2\cosh\,\beta(x\lambda)}, \quad (14)$$

where J represents the number density of micelles through an average number N_v of neighbours to a given micelle by $J=(9/8)N_v$. The order parameters are given by

$$m=1-\frac{3}{2}\int p(\lambda)d\lambda \frac{2\cosh\,\beta(x\lambda)}{e^{-\beta(y\lambda)}+2\cosh\,\beta(x\lambda)} \quad (15)$$

and

$$q=\frac{3}{2}\int p(\lambda)d\lambda \frac{2\sinh\,\beta(x\lambda)}{e^{-\beta(y\lambda)}+2\cosh\,\beta(x\lambda)}. \quad (16)$$

We must solve Equations (13) and (14) for x and y and insert these into Equations (15) and (16) in order to establish the different phases of the system. Phase stability is verified by the calculation of free energies.

For a system of identical particles (a monodisperse system), $p(\lambda)$ turns out to be a simple delta function centred at some λ_0, and x and y (Equations (13)–(14)) can be directly related to the order parameters m and q (Equations (15)–(16)), through $m=-y/2J\lambda_0$ and $q=3x/2J\lambda_0$. In such cases, it can be seen by inspection that the zero temperature solutions are uniaxial ($x=0$) and biaxial behaviour is absent, as expected.

In the case of a dispersive distribution of quadrupoles, and consequently of forms, there is no direct relation between the variables x, y and the order parameters. Note that there is an analogous situation with respect to the relation between the microscopic tensor order parameter $\widetilde{\mathbf{S}}$ and the macroscopic order parameter $\widetilde{\mathbf{Q}}$ (related to the susceptibility), in the case of flexible molecules, for thermotropic liquid crystals (*28, 53*).

4. Phase diagrams

The Gaussian distribution case was already considered (*44*) and we now compare its results with the bimodal distribution. The null dispersion case will also be discussed.

4.1. *Mean-field results*

The phase diagrams for the Gaussian and bimodal distributions are entirely analogous, both displaying a stable biaxial phase and a Landau point with $\lambda_0=0$ (null anisometry) at the same temperature $T_L=9\sigma_0^2/2k_B$, as shown in Figure 3. We have defined dimensionless temperature $t=4k_BT/9N_v\sigma_0^2$ and quadrupole $d=\lambda_0/\sigma_0\sqrt{2}$, so that $t_L=1/3$ and $d_L=0$ are at the Landau point for both distributions.

The fact that the single and bimodal distributions yield the same phases is an important result, because the delta bimodal model is much simpler to handle than the Gaussian distribution, and thus serves very well as a first approximation. Moreover, the two distributions interpolate between two limiting situations: a single Gaussian and two Gaussians of null dispersion, as illustrated in Figure 2. This implies that the intermediate cases (top right and bottom) should also present a biaxial phase.

The mean-field critical biaxial–uniaxial lines near the Landau point can be obtained from an expansion in the biaxial order parameter q, from Equations (13) and (16). They are given, in terms of a measurable Kelvin critical temperature T_c, by

$$T_c=T_L\left[1-\kappa\lambda_0^{2/3}+o\left(\lambda_0^{4/3}\right)\right], \quad (17)$$

where κ is a function of the moments of the distributions of quadrupoles, $\Delta_j=\overline{(\lambda-\lambda)^j}$, and is given by $\kappa\equiv(5\Delta_2/\Delta_6)^{1/3}\Delta_4/9\Delta_6$. Thus, the Gaussian and the delta bimodal cases present slightly different coefficients κ. The uniaxial phases N_C (cylindrical) and N_D (discotic) are present in the regions of positive and negative mean quadrupoles, respectively, corresponding to predominance of disc-like micelles in the discotic phase and of cylinder-like aggregates in the cylindrical phase. The use of the original model of continuous $\widetilde{\mathbf{n}}_i$ directions would lead us to the same basic results, with a slight change in the prefactors of Equation (17), meaning that the biaxial phase would be achieved with a lower energy cost than that

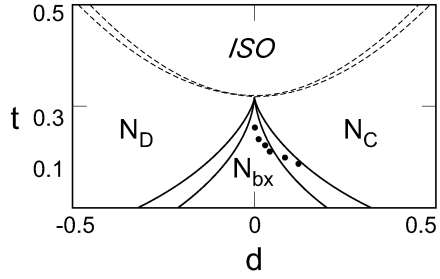

Figure 3. Mean-field theoretical phase diagrams for Gaussian and delta bimodal distribution of quadrupoles. The parameters t and d are explained in the text. A biaxial phase N_{bx} separates a cylindrical N_C from a discotic N_D phase. Solid lines represent critical transitions, with lower transition temperatures for the delta bimodal distribution, and dashed lines stand for the nematic–isotropic lines, with lower transition temperatures for the Gaussian distribution. Dots represent Monte Carlo simulation results for critical N_{bx}–N_C line.

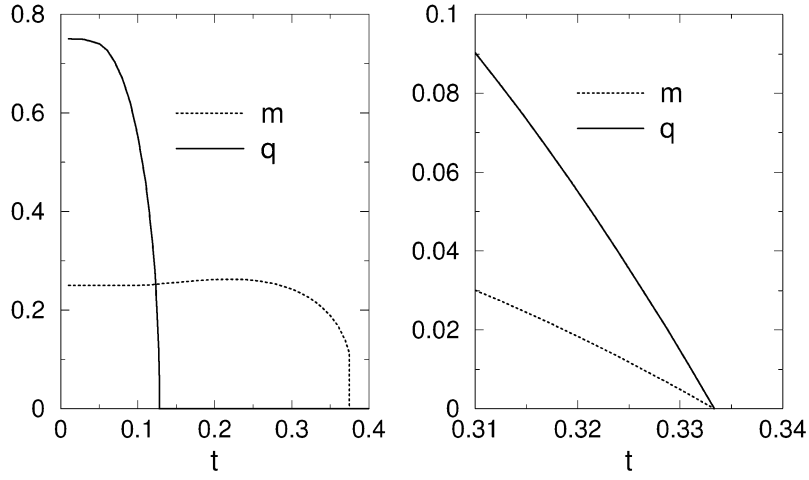

Figure 4. Mean-field order parameters m and q (Equations (15) and (16)) as functions of temperature for small positive anisometry (d=0.2) and near the Landau point for null average anisometry (d=0).

imposed by the discretisation procedure adopted. Note that for the bimodal case, the biaxial phase is restricted to the region $|\lambda_0|/\sigma_0<1$, which is the condition of mixture for this distribution. As for the Gaussian case, mixture is always a possibility, for arbitrary λ_0/σ_0.

The behaviours of the mean-field order parameters m and q, as functions of temperature, are presented in Figure 4, for small positive anisometry (left) and near the Landau point for null average anisometry $\lambda_0=0$ (right). In the first case (left), we have a continuous N_{bx}–N_C phase transition at a lower temperature and a first-order N_C–ISO transition at a higher temperature. In the second case (right), both transitions are continuous and take place at the same temperature. Thus, the biaxial order parameter q vanishes continuously, while the uniaxial nematic order parameter m is discontinuous, at the transition, for positive anisometry ($\lambda_0>0$), as in Figure 4 (left). For null average anisometry ($\lambda_0=0$), both parameters (m and q) go to zero smoothly at the Landau temperature, as in Figure 4 (right).

The phase diagram presents no biaxial phase in the case of the null dispersion theta distribution, that is, for a solution of micelles of a single form, as shown in Figure 5. The region $|\lambda|<\lambda^*$ would be physically unavailable, and would correspond to an abrupt change of form at some λ^*, leading to a direct N_C–N_D transition.

4.2. *Results from Monte Carlo simulations*

In order to check that the phase diagram of the polydisperse models is not an artefact of the mean-field approach, we have performed Metropolis Monte Carlo simulations (*56, 57*). We have considered particles of different anisometries distributed randomly on a cubic lattice with periodic boundary conditions. A vectorised version of the Metropolis algorithm (*58*) was developed (*52*). Measurements of "temporal" correlations (*56*) allowed the design of good statistical samples. Preliminary tests showed that the delta bimodal distribution would again give a good representation of the more complex Gaussian distribution (*52*).

We have thus undertaken detailed simulations for the bimodal distribution, for cubic lattice sizes L=6, 10, 16, 18, 20, with $L(L-1)^2$ micelles. The starting point in all simulations is to settle a distribution of micelles according to the bimodal distribution in each site, and it was observed that different choices for this distribution led to close results, so very few different distributions were needed. For an L=10 lattice, in which the results were observed to be close to an infinite-sized lattice, thermal equilibrium from different starting orientational configurations took about 100 to 400 Monte Carlo steps to be achieved, one Monte Carlo step corresponding to

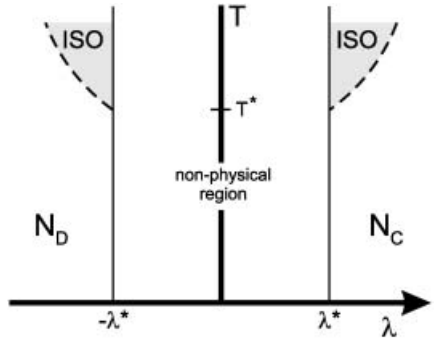

Figure 5. Sketch of the theoretical phase diagram for a null dispersion distribution, the theta distribution, displaying a non-physical region of quadrupoles and two uniaxial N_C and N_D phases.

a full sweep through the whole lattice. Characteristic correlation times were measured to be of the order of 10 Monte Carlo steps, and typical runs were of 10,000 Monte Carlo steps, with the first 1000 discarded.

Simulation data for the N_{bx}–N_C transition line, obtained from the study of fluctuations of the biaxial order parameter q (see (*56, 57*)), are presented in Figure 3, for comparison with mean-field results, for an $L=10$ lattice. Five different distributions of micelles were used at the Landau point, whereas only two were needed for the other points of the uniaxial–biaxial transition. The overall number of measurements for each point was 10 for the Landau point and 6 for the other transition points. The infinite lattice Landau point temperature obtained from finite-size scaling analysis (*56*) is $t=0.238$, lower than the value 1/3 of the mean field, as expected. The order parameters in the biaxial region are obtained from the simulations and shown in Figure 6 for null average anisometry and $L=10$.

5. Comparison with experiment

In this section, we compare our theory with experiment by direct adjustment of our model parameters with experimental phase diagrams. First we analyse diagrams with biaxial phases, as is the case of the KL/water/decanol system, and then the possibility of coexistence of uniaxial phases, as in the system SDS/water/decanol.

5.1. *Biaxial phases*

We propose a comparison of the experimental phase diagram of Yu and Saupe (*6*), with the theoretical prediction of Figure 3, near the Landau point. The

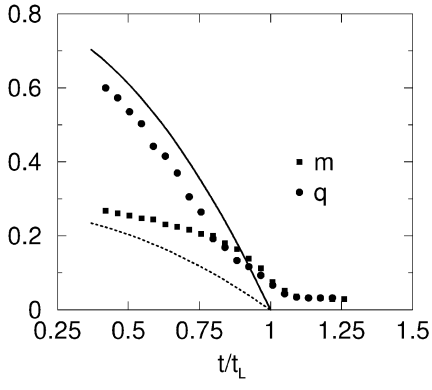

Figure 6. Order parameters m and q (Equations (11) and (12)) from Monte Carlo simulations for a cubic lattice with $L=10$ compared with mean-field results for null average anisometry $\lambda_0=0$. Monte Carlo infinite lattice Landau temperature is $t_L=0.238$ from finite size scaling. Dotted (m) and solid lines (q) represent mean-field results near the Landau point. The mean-field Landau temperature is $t_L=1/3$.

strong asymmetry with respect to the N_C and N_D phases of the experimental phase diagram can be dealt with through an expansion, up to first order, of λ_0 into powers of KL fractional weight concentration, $P_{surf}=P_{KL}$, and temperature T, that reads

$$\frac{\lambda_0}{\sigma_0} = a\Delta p + b\Delta t, \tag{18}$$

with $\Delta p \equiv \left(P_{KL} - P_{KL}^{L}\right)/P_{KL}^{L}$ and $\Delta t \equiv (T^{L}-T)/T_L$, the distances in laurate concentration and temperature from the Landau point. We take experimental points to find a and b adjusting Equation (18) by comparison with the theoretical critical lines given by Equation (17). The experimental points taken for the fitting are $L=\left(P_{KL}^{L}=0.2619,\ T^{L}=317\right)$ (Landau point), $B=(0.2596, 307)$ (a cylindrical-biaxial point), and a point on the discotic-biaxial line, $A=(0.2577, 307)$ (see (*6*)). Our comparison must not be extended to low-temperature phases, as implicit in the above expansion, which cannot account for the inversion of behaviour with concentration observed below 30°C.

We can find a and b for the dispersive Gaussian and delta bimodal distribution, both of which lead to biaxial phases. We adopted the mean number of neighbours $N_v=6$ for numerical purposes, and we found that comparison with experiment is essentially unaffected by different choices. For the Gaussian distribution, the fitting gives $a_G \simeq 1.26$ and $b_G \simeq 0.50$, where G stands for Gaussian. The same procedure yields $a_\Delta \simeq 2.18$ and $b_\Delta \simeq 0.86$ for the delta bimodal case, showing that the delta bimodal distribution leads to larger coefficients. Comparison between theory and experiment is shown in Figure 7. The Gaussian and bimodal descriptions are indistinguishable near the Landau point and the phase transition lines coincide on the scale of the Figure. The two distributions also differ in shape population variations. For the double delta distribution, populations of cylinders and discs are fixed at 50%, while only quadrupoles change. As for the Gaussian case, we find equal populations only very close to a bissecting line inside the biaxial region crossing the Landau point. Above this line we have population predominance of discs and below predominance of cylinders. Population variation along the diagram is expected as long as we accept the system as polydisperse, although a bimodal distribution, of which the double delta is a simplified representation, may be considered a more realistic description of micellar form change.

The comparison of the critical lines from theory to experimental points allows coexistence lines to be drawn without further fitting. The nematic–isotropic lines can be drawn from the approximate expression

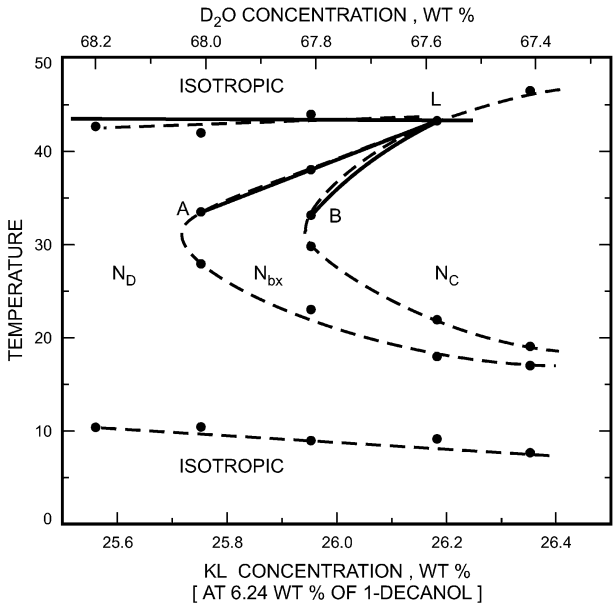

Figure 7. Experimental phase diagram by Yu and Saupe (*6*) (dashed lines) compared with theory (solid lines). Here N_C and N_D are as in Figure 1, L is the Landau point, N_{bx} is the biaxial phase and A and B are the fitting points as explained in the text.

$T = 317 + 4.353 \times 10^{23}\lambda_0^2$, for phase coexistence, as imposed by the theory, and result as almost straight, as a consequence of the smallness of λ_0 (of order of 10^{-14}) obtained by application of Equation (18). Note that the predicted transition lines compare well to the experiment, particularly for the N_D–ISO coexistence.

Biaxiality of the model system is described by properties of the tensorial order parameter $\widetilde{S}$ (Equation (10)). However, strict comparison with experiment is not possible, for reasons we explain below.

The presence of biaxiality has been described for lyotropic systems in terms of related quantities, obtained from NMR and from different susceptibility experiments. In NMR, the electric field gradient tensor on deuterium, taken as uniaxial in the reference frame of the O–D bond (*6*), displays biaxiality in the phase reference frame, if the phase is biaxial (*29, 41*). A biaxiality parameter η is obtained from NMR quadrupolar splittings, which depend on the field gradient components q_{ij}, referred to as the phase symmetry axes, through $\eta = (q_{xx} - q_{yy})/q_{zz}$, with $|q_{zz}| > |q_{yy}| > |q_{xx}|$. The electric field gradient tensor q_{ij} is proportional to the ordering matrix S_{ij}^{O-D} for the O–D bond, because the unaveraged quadrupolar tensor has cylindrical symmetry about this bond (*10, 28*), yielding $\eta_{O-D} = \left(S_{xx}^{O-D} - S_{yy}^{O-D}\right) \Big/ S_{zz}^{O-D}$ for the elements of the O–D ordering matrix.

Alternatively, the ratio of NMR splittings, r, with $r_{O-D} = v(90^\circ)/v(0^\circ)$, may be obtained under rotation of samples, yielding the ratio $S_{zz}^{O-D} \Big/ S_{yy}^{O-D}$ (see (*6*)). Heavy water used as a probe in deuterium NMR spectroscopy forms an essential component of the lyotropic biaxial nematic. Therefore, in order to compare the biaxiality parameter, which comes out of the NMR experiment, η_{O-D}, and that which results from our theory, $\eta = (S_{xx} - S_{yy})/S_{zz}$, additional modelling of water distribution on the uniaxial particles which represents micelles would be required. Since such modelling has not been a goal of our work, the comparison we present below is strictly speculative in nature.

In parallel to NMR results, experimental data on different susceptibility properties may be organised conveniently in terms of the symmetric al invariants of the experimental tensor macroscopic order parameter $\widetilde{Q}$ (see (*8, 42*)). One of them, σ_3, defined as $\sigma_3 = 4Q_{xx}Q_{yy}Q_{zz}$, is particularly useful in identifying a biaxial phase.

In order to further explore our model properties, we undertake two simplifying assumptions of qualitative nature: (i) we assume a tensor macroscopic order parameter $\widetilde{Q}$ comparable to the model microscopic order parameter $\widetilde{S}$, so we make $\sigma_3 = 4S_{xx}S_{yy}S_{zz}$; (ii) we further take $\widetilde{S}$ and $\widetilde{S_{O-D}}$ as comparable. As a consequence of (ii), $r = S_{zz}/S_{yy}$ is comparable to r_{O-D}. Thus, η and $\widetilde{\sigma_3} = \sigma_3 \big/ S_{zz}^3$, which behaves as σ_3, may be obtained from r. In Figure 8, we present model calculation curves for the three parameters r, η and σ_3, as functions of temperature, at $P_{KL} = 0.2595$. The sign inversion of σ_3 on crossing a biaxial region has also been found in low-temperature regions of the diagram, distant from the Landau point, in which σ_3 was directly measured in terms of the dielectric susceptibility tensor (*8, 42*). Maximum biaxiality is too high for the mean-field case, as usual, owing to the approximations involved, which neglect fluctuations, as illustrated by the lower value shown by Monte Carlo results.

Experimental values for the three parameters at $P_{KL} = 0.2595$ are also shown: values for r_{O-D} (top of Figure 8), are taken from Yu and Saupe's work (*6*) and values for $\widetilde{\sigma_3}$ and η (bottom left and bottom right of Figure 8) are calculated from r_{O-D}. It should be noted that the absence of a model relating O–D bonds to the micellar orientations, which would make theory really comparable to experiment, may be the most important reason behind the discrepancies noted inside the biaxial region.

The use of a non-symmetric anisometry distribution would lead to smoother theoretical curves, particularly inside the biaxial region. For a continuous distribution of the possible orientations of the micellar axes, as opposed to the discrete distribution of possible orientations adopted in this study, the

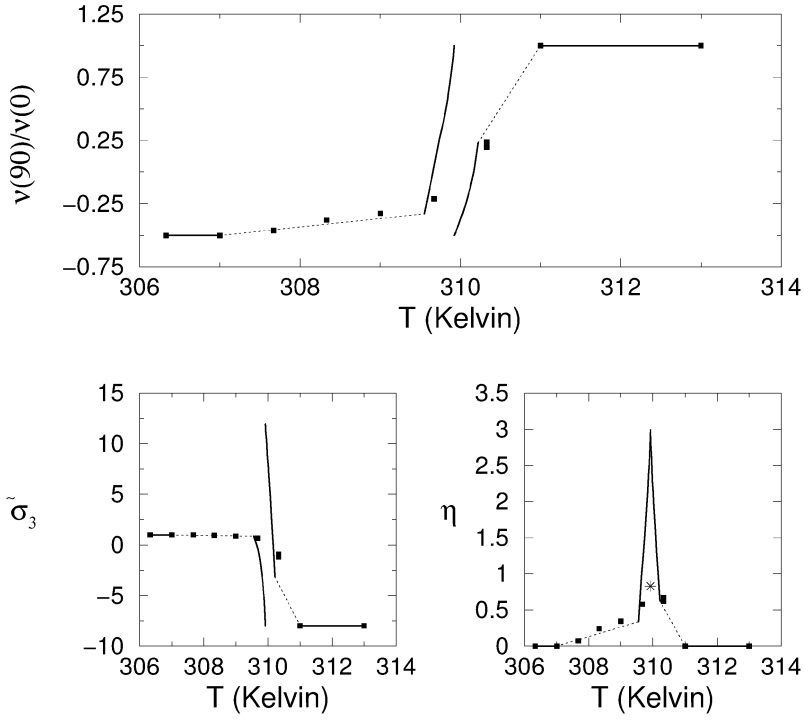

Figure 8. Model biaxiality parameters (lines for mean-field, stars for Monte Carlo), calculated from the ordering matrix $\widetilde{S}$ (Equation (10)), at $P_{KL}=0.2595$. Top graph is r, in the $\nu(90^\circ)/\nu(0^\circ)$ axis. Bottom graphs are $\widetilde{\sigma_3}$ (left) and η. See the text for definitions. Dashed lines represent regions of numerical instabilities in mean-field calculations. For illustration, experimental points of $\nu(90^\circ)/\nu(0^\circ)$ from Yu and Saupe's paper (*6*) are plotted in the top graph. Data for $\widetilde{\sigma_3}$ and η, calculated from experimental values of r_{D-O}, under particular assumptions described in the text, are also shown. Experimental data are represented as squares.

numerical values of the calculated parameters might change slightly, but overall behaviour would not suffer qualitative change.

5.2. *Uniaxial nematic coexistence*

Interpretation of the quadrupole distribution of case (iii) may be as follows. We use λ^* to represent the absolute value of quadrupoles at the surfactant concentration $P_{surf}=P^*$ at which the change of symmetry takes place, that is, at which micelle form changes from disc ($\lambda<0$) to cylinder ($\lambda>0$). We thus may assume the dependence of form on concentration and write linear expansions:

$$\lambda_{c,\,d} = \pm\lambda^* + \alpha_{c,\,d}\Delta P_{surf} \qquad (19)$$

with $\Delta P_{surf}=P_{surf}-P^*$.

The $T-P_{surf}$ phase diagram presents two uniaxial phases with a form coexistence at P^*. This coexistence line ends at a point ($P_{surf}=P^*$, $T=9(\lambda^*)^2/16k_B\ln 2$). At this point the two uniaxial phases coexist with the isotropic phase. Figure 9 shows the corresponding phase diagram. Note that differently the from the previous case, in which a biaxial region is possible, the coexistence end point is not critical. Such behaviour is presented by SDS/water/decanol (*27, 35*).

6. Tests for a microscopic micellar model near the Landau point

In order to give a microscopic interpretation for micellar change of form, we consider the micellar geometries and, in accordance with proposals present in the related literature, the corresponding partition of decanol and laurate (*43*), as well as chain

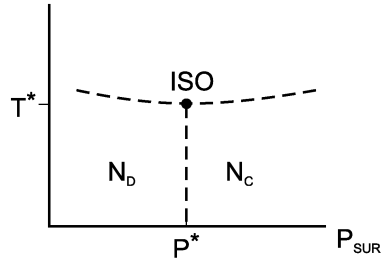

Figure 9. Sketch of an experimental phase diagram corresponding to the discontinuous quadrupole distribution, the theta distribution, displaying no biaxial phase and direct N_C–N_D transition at a surfactant concentration P^*.

contraction (*59*). We add specific assumptions for micelle volume and relative density at the Landau point. Our approach is as follows: (i) we model micelle geometry as represented in Figure 1; (ii) we model decanol as going preferentially to surfaces of less curvature, also represented in Figure 1; (iii) we relate quadrupoles to geometric parameters; (iv) we assume equal micelle volumes and surfactant/cosurfactant densities at the Landau point; (v) we include chain contraction under increasing temperature. This procedure is developed in Equations (20)–(28) and allows description of anisometry behaviour with temperature and relative concentration, given in Equations (29) and (30).

We first separate λ_0 as an average representing cylindrical shapes with quasi-quadrupoles λ_c and average discotic shapes with λ_d, to introduce explicit form dependence in the average quadrupole expressions and make the Gaussian description closely related to a more realistic bimodal quadrupole distribution. So we write

$$\lambda_0 = f_d\lambda_d + f_c\lambda_c, \tag{20}$$

with $f_{c,d}$ corresponding to the fractions of cylinders and discs in the mixture. Here $f_{c,d}$ are calculated taking λ_0/σ_0 to be small, near the Landau point. The picture we propose is illustrated in Figure 10. Considering the Gaussian distribution case and Equation (18) we obtain

$$\lambda_{c,\,d}/\sigma_0 = \pm\sqrt{2/\pi} + a_G\Delta p + b_G\Delta t, \tag{21}$$

with $a_G>0$ and $b_G>0$. The implications are that positive quadrupoles, associated with cylinders, increase with laurate concentration P_{KL} ($\Delta p>0$) and decrease with temperature T ($\Delta t<0$) as we move from the Landau point. As for negative quadrupoles, associated with disc-like objects, their absolute values decrease with P_{KL} and increase with temperature.

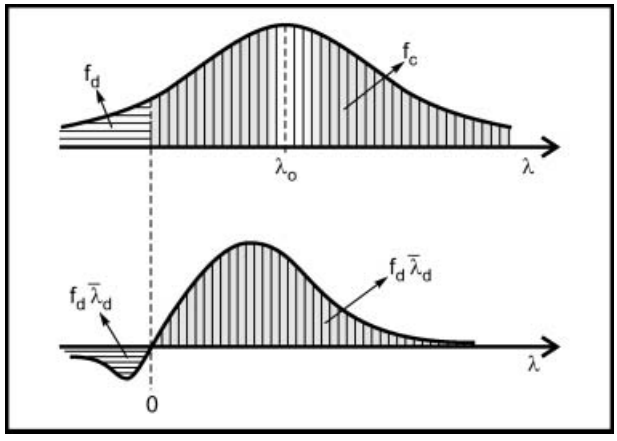

Figure 10. Top: qualitative graphical representation of the distribution $p(\lambda)$ of quadrupoles, with areas divided into fractions of discs, f_d, and cylinders f_c. Bottom: graph of the function $\lambda p(\lambda)$. Areas represent mean disc $(f_d\bar{\lambda}_d<0)$ and cylinder $(f_c\bar{\lambda}_c<0)$ quadrupoles.

We now write quadrupoles λ_c and λ_d as functions of micellar geometrical parameters. This was done considering that the intermicelle potential may be taken as suggested previously by a DLVO model study (*54*). The quadrupoles λ_i, resulting from a multipole expansion of this potential, will be integrals depending on some internal micellar density and on the geometries of the micelles, given by Figure 1. By imposing constant mean linear chain length l, rounded discs will have fixed height H and spherocylinders will have a fixed diameter D. Taking $v\equiv H/D$, we have

$$\lambda_c = K_c\left(v_c^2 + v_c^3\right) \tag{22}$$

for the spherocylinders, and

$$\lambda_d = -K_d\left(\frac{\pi}{4v_d} + \frac{1}{3v_d^2} + \frac{\pi}{8v_d^3} + \frac{1}{8v_d^4}\right) \tag{23}$$

for the rounded discs. Here, v_c and v_d are related to the anisometries μ_c and μ_d, defined as the ratio of the largest to the lowest linear dimension for each correspondent micelle, by $\mu_c=v_c+1$ and $\mu_d=(v_d+1)/v_d$.

Expressions (22) and (23) for λ_c and λ_d must be compared with Equation (21) for microscopic interpretation of the quasi-quadrupoles dependence on relative concentration P_{KL} and temperature T. To achieve this aim, we must first obtain the micellar anisometries, K_c and K_d, at the Landau point. The anisometries at the Landau point were calculated with a partition model of surfactant and cosurfactant in each form, as in previous studies (*36, 55*). The global paraffinic volume of the hydrocarbon chains in the micelle will be divided into V_{pure}, corresponding to the part in which there is only laurate, and V_{mix}, where decanol is also present. Molecular volumes of decanol and laurate are, respectively, v_{dec} and v_{KL}. Here, N_{dec} is the number of decanol molecules per micelle, and the number of laurate molecules, N_{KL}, is divided into two parts, with $(N_{KL})_{pure}$ corresponding to the part of the micelle in which there is only laurate, and $(N_{KL})_{mix}$ to the part in which there is a mixture of decanol and laurate. We then define the ratio $r\equiv V_{pure}/V_{mix}$ for either of the geometries of Figure 1. These ratios can also be written assuming (*43*) that the decanol molecules are located on the surfaces of less curvature, plane areas

of rounded discs and bodies of spherocylinders, with the corresponding volumes constituting V_{mix}. Assuming the ratio of the number of KL to decanol molecules per micelle, N_{KL}/N_{dec}, to be the same as [KL]/[dec] that prevails in the solution, we obtain

$$v_c = \frac{2}{3}\frac{\gamma_c + \alpha}{P_{KL}/\varepsilon - \gamma_c}, \tag{24}$$

for the spherocylinders, and

$$v_d = -\frac{3\pi}{8} + \frac{1}{2}\sqrt{\frac{9\pi^2}{16} + 6\left(\frac{P_{KL}/\varepsilon - \gamma_d}{\gamma_d + \alpha}\right)}, \tag{25}$$

for the rounded discs, invoking standard geometrical formulae for the needed volumes. In these Equations, $\gamma \equiv (N_{KL})_{mix}/N_{dec}$ and $\varepsilon = 0.10742$ stands for the conversion of KL molar fraction units into percentage weight units of the experiment. We obtained $\alpha \equiv v_{dec}/v_{KL} \simeq 0.9168$, with v_{dec} and v_{KL} given by $v = 27.4 + 26.9n$ (see (*60, 61*)), for chain volumes containing n carbon atoms in the micelle. We have $n = 11$ for KL, since the 12th carbon is in the polar head, and $n = 10$ for decanol.

We impose the paraffinic volumes and number of decanol or laurate molecules of different shapes to be equal at the Landau point, as expected from a single micelle changing its form. These two latter conditions will lead us to

$$v_c^L = \left(v_d^L\right)^{-2} + \pi\left(2v_d^L\right)^{-1}, \tag{26}$$

and

$$\frac{v_c}{v_{dec} + v_{KL}\gamma_c} = \frac{1}{v_d^2(v_{dec} + v_{KL}\gamma_d)}. \tag{27}$$

The solution of the Equations (24)–(27) for v_c, v_d, γ_c and γ_d, at the Landau point, yields $v_c^L = 2.57$, $v_d^L = 1.00$, $\gamma_c^L = 1.74$, $\gamma_d^L = 0.119$. From the numbers above we obtain $\mu_c^L = 3.57$ and $\mu_d^L = 2.00$, in reasonable agreement with known values at the phase transition (*36*). Finally, going back to (22) and (23), we get $K_c^L = 1.054 \times 10^{-12}$ and $K_d^L = 1.52 \times 10^{-11}$ at the Landau point.

We now extend the calculations to the region near to the Landau point, taking into account the chain length dependence of $K_{c,d}$. Using $K_{c,d} \sim l^5$, by dimensional analysis of the quadrupole integrals, and the chain thermal contraction coefficient, $(1/l)(\partial l/\partial T) \simeq -1.6 \times 10^{-3} K^{-1}$ (see (*59*)), we obtain

$$K_{c,d} = K_{c,d}^L(1 + 2.536\Delta t), \tag{28}$$

with $K_{c,d}^L$ being the Landau point values. Chain volume has been regarded as constant, owing to its small positive coefficient (*59*). Now we use Equations (21), (22) and (23) to obtain the anisometry dependence on the experimental variables, taking into account the dependence of $K_{c,d}$ on temperature, as in Equation (28). We obtain

$$\mu_c = 3.57 + 1.93\left(P_{KL} - P_{KL}^L\right) - 6.38 \times 10^{-3}\left(T^L - T\right) \tag{29}$$

and

$$\mu_d = 2.00 - 1.06\left(P_{KL} - P_{KL}^L\right) - 4.22 \times 10^{-3}\left(T^L - T\right). \tag{30}$$

Anisometry behaviour predicted by Equations (29) and (30) may be rationalised as follows: (i) both micellar shapes become less anisometric as temperature is lowered, and this behaviour is expected under chain expansion, since disc height and cylinder radius increase; (ii) as to laurate concentration, P_{KL}, its increment makes cylinders grow and discs shrink, in accordance with the neighbouring nematic phase behaviour along the diagram, hexagonal and lamellar.

An additional result may also be derived with respect to aggregate volumes. From geometric formulae and (29)–(30) we obtain

$$V_c/V_c^L = 1.00 + 0.595\left(P_{KL} - P_{KL}^L\right) + 2.83 \times 10^{-3}\left(T^L - T\right) \tag{31}$$

and

$$V_d/V_d^L = 1.00 - 1.75\left(P_{KL} - P_{KL}^L\right) + 0.145 \times 10^{-3}\left(T^L - T\right), \tag{32}$$

for hydrocarbon volume variations along the phase diagram, with $V_{c,d}^L$ representing Landau-point volumes. Here $V_{c,d}^L$ are calculated taking laurate molecules to define chain length from $l = 1.5 + 1.265n$, for n CH_2 groups of the extended hydrocarbon tails at 10°C (gel phase) (*60, 61*), and the chain thermal contraction coefficient. This leads us to micelles of about 200 molecules at the Landau point. Our results indicate micellar aggregation number variation following volume changes, as a consequence of fixed chain volumes. Micelles of either shape have increasing volumes as the temperature is lowered, with cylinders increasing much faster than discs. The effect of laurate concentration is opposite on cylinders and discs, as expected.

Note that fixed volumes, implying fixed aggregation numbers, for a concentration at the Landau point value, would yield

$$\mu_c = 3.57 - 15.5 \times 10^{-3}\left(T^L - T\right) \tag{33}$$

and

$$\mu_d = 2.00 - 4.35 \times 10^{-3}\left(T^L - T\right). \tag{34}$$

Comparison of Equations (29) and (30) with (33) and (34) with fixed concentration imply that discs practically do not change their aggregation number, whereas cylinders suffer a rapid decline in aggregation number as temperature is increased.

7. Final comments

Our theory suggests the relation of biaxial phases in lyotropes, as in (*6*), to a smooth uniaxial micelle form transition. Also, the direct lyotropic N_D–N_C transition, as in (*35*), is consistent with an abrupt change of shape of uniaxial micelles. In the case of a smooth form transition, the biaxial phase is present for a whole range of possible distributions, from single Gaussian to bimodal distribution. Different from other model mixtures considered in the literature, biaxiality results from the homogeneous mixture of uniaxial form in the exchange condition.

In the case of a smooth transition model, fitting of the theoretical critical lines to experimental data of Yu and Saupe allows the prediction of first-order transition lines in good agreement with experiment. The coexistence line is especially good for the N_D–ISO transition. An asymmetrical distribution of forms, represented through $p(\lambda)$, which could mimic a stronger increase in cylinder population in the N_C phase, could explain the discrepancy in the adjusted ISO–N_C line. The fitting procedure for the critical lines also permits calculation of system biaxiality in close accordance with experimental data.

A geometrical and decanol partition model for micelles, associated with the fitting parameters, displays physically consistent microscopic parameters, such as anisometries (μ), local relative densities (γ) and aggregation numbers. The competition between temperature effects on the hydrocarbon chains and micellar aggregation produce a smaller variation of anisometry than would be expected from chain length variation alone, in the case of cylinders. This would explain the features of the phase diagram for temperatures above 30°C.

Our study also allows a reinterpretation of the results of neutron scattering on the KL/decanol/water system, for an uniaxial phase in the proximity of the biaxial phase (*62*). From the asymmetry in the detected distribution of decanol and laurate molecules in the plane perpendicular to the director, Hendrikx *et al.* (*62*) suggest the existence of different curvatures in that plane, giving an indication of the biaxiality of the micelles. However, a different interpretation is possible. In the case of an N_C phase, a mixture of (larger) cylinders and (smaller) discs and local perpendicular alignment of the disc symmetry axes would imply more decanol in the direction parallel to disc surfaces and less curvature and less decanol in the direction perpendicular to disc surfaces. However, because the alignment of discs is only local, in micro regions, the overall phase is uniaxial.

Finally, in light of our study, we suggest an interpretation for the lower temperature part of the phase diagram (below 30°C). The sequences of phases can be understood, from a qualitative point of view, from the variations of the micellar object with temperature and concentration. Hydrocarbon chains are characterised by chain length contraction with increasing temperature, and this effect has been invoked previously to explain the re-entrant nematic phase (*34*). It should be stressed that such contraction, expressed by a negative temperature coefficient, holds only in the chain direction. The paraffin volume as a whole has a small positive temperature coefficient (*59*). Therefore, while the direction of the chain is contracting with increasing temperature, the other directions are expanding, conserving the whole paraffin volume at a practically constant level over the temperature range of interest, when the number of molecules in the micelles does not change. This would imply that cylinders and discs are more anisotropic with increasing temperature.

In a cylinder, two dimensions are contracting while in discs only one dimension is contracting with temperature. Therefore, cylinders grow faster with increasing temperature, given the same chain contraction. As a consequence, the population of forms, as well as average quadrupoles, have distortions as a function of temperature. The N_D–N_{bx}–N_C transition observed with increasing temperature in the lower part of the phase diagram for $P_{KL}>0.26$ is, in fact, expected if the volumes and aggregation numbers of micelles remain constant with temperature. So the full sequence observed with increasing temperature at $P_{KL}\sim0.26$, N_D–N_{bx}–N_C–N_{bx}–N_D can be rationalised by an initially constant aggregation number, with increasing anisometries, followed by a combination of yet increasing anisometries but decreasing aggregation numbers, by thermal agitation and excluded volume effects. This accounts for the re-entrant behaviour of the N_C and N_{bx} domain in the N_D phase. Note also that, as we reach lower temperatures, chain

expansion is more favourable to less curved areas and disc growth.

Acknowledgements

The authors are grateful to the Brazilian agencies CNPQ, FAPESP, FAPERGS and CAPES for financial support. Monte Carlo simulations were performed at CESUP (Centro de Supercomputação da UFRGS). EFH thanks P. R. Krebs for helpful discussions and technical support concerning Monte Carlo simulations, Y. Levin for a brief discussion concerning micelle–micelle interaction mechanisms and P. S. Kuhn for reading the proofs.

References

(1) Amaral L.Q.; Pimentel C.A.; Tavares M.R.; Vanin J.A. *J. Chem. Phys.* **1979**, *71*, 2940.
(2) Charvolin J.; Levelut M.; Samulski E.T. *J. Phys. Lett. (Paris)* **1979**, *40*, L–587.
(3) Forrest B.J.; Reeves L. *Chem. Rev.* **1981**, *81*, 1.
(4) Luzzati V. *Biological Membranes*; Chapman D. (Ed.), Academic Press: New York, 1968. pp. 71–123.
(5) Ekwall P. *Adv. Liq. Cryst.* **1975**, *1*, 1–142.
(6) Yu L.J.; Saupe S. *Phys. Rev. Lett.* **1980**, *45*, 1000.
(7) Figueiredo Neto A.M.; Galerne Y.; Levelut A.M.; Liebert L. *J. Phys. (Paris) Lett.* **1985**, *46*, L499.
(8) Galerne Y.; Figueiredo Neto A.M.; Liebert L. *J. Chem. Phys.* **1987**, *87*, 1851.
(9) Luckhurst G.R. *Nature* **2004**, *430*, 413.
(10) Severing K.; Saalwächte K. *Phys. Rev. Lett.* **2004**, *92*, 125501.
(11) Madsen L.A.; Dingermans T.G.; Nakata M.; Samulski E.T. *Phys. Rev. Lett.* **2004**, *92*, 145505.
(12) Acharya B.R.; Primak A.; Kumar S. *Phys. Rev. Lett.* **2004**, *92*, 145506.
(13) Merkel K.; Kocot A.; Vij J.K.; Korlacki R.; Mehl G.H.; Meyer T. *Phys. Rev. Lett.* **2004**, *93*, 23781.
(14) Freiser M.J. *Phys. Rev. Lett.* **1970**, *24*, 1041.
(15) Straley P.J. *Phys. Rev. A* **1974**, *10*, 1881.
(16) Shih C.S.; Alben R.J. *J. Chem. Phys.* **1972**, *57*, 3057.
(17) Alben R. *Phys. Rev. Lett.* **1973**, *30*, 778.
(18) Alben R. *J. Chem. Phys.* **1973**, *59*, 4299.
(19) Palffy-Muhoray P.; de Bruyn J.R.; Dunmur D.A. *J. Chem. Phys.* **1985**, *82*, 5294.
(20) Sharma S.R.; Palffy-Muhoray P.; Bergersen B.; Dunmu D.A. *Phys. Rev. A* **1985**, *32*, 3752.
(21) van Roij R.; Mulder B. *J. Phys. II France* **1994**, *4*, 1763.
(22) Martinez-Ratón Y.; Cuesta J.A. *Phys. Rev. Lett.* **2002**, *89*, 185701.
(23) Galindo A.; Haslam A.J.; Varga S.; Jackson G.; Vanakaras A.G.; Photinos D.J.; Dunmur D.A. *J. Chem. Phys.* **2003**, *119*, 5216.
(24) Landau L.D. *Collected Papers*; Ter Haar D. (Ed.), Gordon and Breach: New York, 1965.
(25) Gramsbergen E.F.; Longa L.; de Jeu W. *Phys. Rep.* **1986**, *135*, 195.
(26) Longa L.; Pajak G. *Liq. Cryst.* **2005**, *32*, 1409.
(27) Amaral L.Q. *Liq. Cryst.* **1990**, *7*, 877.
(28) de Gennes P.G. *The Physics of Liquid Crystals*; Clarendon Press: Oxford, 1974.
(29) Luckhurst G. *Thin Solid Films* **2001**, *40*, 393.
(30) Galerne Y.; Marcerou J.P. *Phys. Rev. Lett.* **1983**, *51*, 2109.
(31) Longa L.; Grzybowski P.; Romano S.; Virga E. *Phys. Rev. E* **2005**, *71*, 051714.
(32) Bates M.A.; Luckhurst G.R. *Phys. Rev. E* **2005**, *72*, 051702.
(33) Taylor M.P.; Herzfeld J. *Phys. Rev. A* **1991**, *44*, 3742.
(34) Oliveira M.J.; Figueiredo Neto A.M. *Phys. Rev. A* **1986**, *34*, 3481.
(35) Amaral L.W.; Helene M.E.M. *J. Phys. Chem.* **1988**, *92*, 6094.
(36) Amaral L.Q.; Santin Filho O.; Taddei G.; Vila Romeu N. *Langmuir* **1997**, *13*, 5016.
(37) Teixeira C.V.; Itri R.; Amaral L.Q. *Langmuir* **2000**, *16*, 6102.
(38) Quist P.O. *Liq. Cryst.* **1995**, *18*, 623.
(39) Ho C.; Goetz R.J.; Elaaser M.S. *Langmuir* **1991**, *7*, 630.
(40) Mello Filho A.A.; Laverde A.; Fujiwara F.Y. *Langmuir* **2003**, *19*, 127.
(41) Nicoletta F.P.; Chidichimo G.; Goleme A.; Picci N. *Liq. Cryst.* **1991**, *10*, 665.
(42) Santoro P.A.; Sampaio A.R.; da Luz H.L.F.; Palangana A.J. *Phys. Lett. A* **2006**, *353*, 512.
(43) Gelbart W.M.; McMullenn W.E.; Madster A.; Ben-Shaul A. *Langmuir* **1985**, *1*, 101.
(44) Henriques E.F.; Henrique V.B. *J. Chem. Phys.* **1997**, *107*, 8036.
(45) Tanford C. *Proc. Natl. Acad. Sci. U.S.A.* **1974**, *71*, 1811.
(46) Israelachvili J.N.; Mitchell D.J.; Ninham B.W. *J. Chem. Soc. Faraday Trans. II* **1976**, *72*, 1525.
(47) Maier W.; Saupe A. *Z. Natursforsch.* **1958**, *13a*, 564.
(48) Ma S.K. *Modern Theory of Critical Phenomena*; W.A. Benjamin: New York, 1976.
(49) Ashcroft N.W.; Mermin N.D. *Solid State Physics*; Saunders College: PhiladelphiaPA, 1976.
(50) Zwanzig R. *J. Chem. Phys.* **1963**, *39*, 1714.
(51) Thompson C.J. *Classical Equilibrium Statistical Mechanics*; Oxford University Press: Oxford, 1988.
(52) Henriques E.R. Ph.D. Thesis, University of Sao Paulo, 1999.
(53) Singh S. *Phys. Rep.* **2000**, *324*, 107.
(54) Amaral L.Q.; Figueiredo Neto A.M. *Mol. Cryst. Liq. Cryst.* **1983**, *98*, 285.
(55) Taddei G.; Amaral L.Q. *J. Phys. Chem.* **1992**, *96*, 6102.
(56) Binder K.; Heerman D.W. *Monte Carlo Simulation in Statistical Physics, An Introduction*; Springer: Berlin, 1992.
(57) Landau D.P.; Binder K. *A Guide to Monte Carlo Simulations in Statistical Physics,* second edition, Cambridge University Press: Cambridge, 2005.
(58) Staufer D.; Hehl F.W.; Ito N.; Winkelmann V.; Zabolitsky J.G. *Computer Simulation and Computer Algebra,* third enlarged edition, Springer: Berlin, 1993.
(59) Luzzati V.; Mustacchi H.; Skoulios A.; Husson F. *Acta Cristalogr* **1960**, *13*, 660.
(60) Tanford C. *J. Chem. Phys.* **1972**, *76*, 3020.
(61) Tanford C. *J. Phys. Chem.* **1974**, *78*, 2469.
(62) Hendrikx Y.; Charvolin J.; Rawis M. *Phys. Rev. B* **1986**, *33*, 3534.